Calibration of Soil Model Parameters Using Particle Swarm Optimization

J. Sadoghi Yazdi[1]; F. Kalantary[2]; and H. Sadoghi Yazdi[3]

Abstract: In this paper, a neuro-fuzzy model in conjunction with particle swarm optimization (PSO) are used for calibration of soil parameters used within a linear elastic-hardening plastic constitutive model with the Drucker-Prager yield criterion. The neuro-fuzzy system is used to provide a nonlinear regression between the deviatoric stress and axial strain ($\sigma_d - \varepsilon$) obtained from a consolidated drained triaxial test on samples of poorly graded sand. The soil model parameters are determined in an iterative optimization loop with PSO and an adaptive network based on a fuzzy inference system such that the equations of the linear elastic model and (where appropriate) the hardening Drucker-Prager yield criterion are simultaneously satisfied. It is shown that the model parameters can be determined with relatively high accuracy in spite of the limited insight gained by a single set of data. To verify the robustness of the technique, a second set of data obtained under different confining pressures is then used in a separate run. The outcome shows a close match with the same order of accuracy. **DOI: 10.1061/(ASCE)GM.1943-5622.0000142.**

CE Database subject headings: Fuzzy sets; Particles; Optimization; Parameters; Soils.

Author keywords: Neuro-fuzzy inference system; Particle swarm optimization; Drucker-Prager yield criterion; Soil parameters.

Introduction

A variety of methods exist for calibration of soil model parameters based on laboratory tests. The optimization method is an important method used in the identification of geotechnical parameters used in constitutive equations. Swarm intelligence approaches are power tools for optimization of cost function. Many research works with a wide range of applications can be found on this subject. Some of these approaches that have direct applications to geomechanics are mentioned here. For the identification of soil parameters Levasseur et al. (2008) used genetic algorithms. Feng et al. (2006) used an inverse technique for the determination of the parameters of visco-elastic constitutive models for rocks based on genetic programming and a particle swarm optimization (PSO) algorithm. Meier et al. (2008) presented a concept for the application of PSO in geotechnical engineering. For the calculation of deformations in soil or rock, numerical simulations based on continuum methods are widely used in the field of geoenvironmental engineering. Schanz et al. (2006) applied PSO techniques to geotechnical field projects and laboratory tests; namely, a multistage excavation and the desaturation of a sand column. Zhao and Yin (2009) presented a method for identification of geomechanical parameters using a combination of a support vector machine, PSO, and numerical analysis techniques. Finsterle (2006) examined the potential use of standard optimization algorithms for the solution of aquifer remediation problems in three-phase and three-component flow and transport simulations of contamination plumes. As a different aspect of parameter identification, Cui and Sheng (2005) determined the minimum parametric distance to the limit state of a strip foundation by optimizing a reliability index.

In this paper, a triaxial test result is used in conjunction with a typical elastoplastic constitutive model to arrive at the model parameters using a PSO algorithm. The paper is organized in four main sections: Introduction, Preliminaries (including the soil constitutive model, PSO algorithm, and neuro-fuzzy model), Proposed Method (including the experimental results), and Summary and Conclusions.

Preliminaries

This section includes a necessary explanation of soil constitutive modeling, the PSO algorithm, and the neuro-fuzzy model.

Soil Constitutive Modeling

The behavior of geologic material may be represented by several classes of constitutive models, such as variable moduli and hyper-elasic, hypoelastic, endochronic, and plasticity formulations (Chen 1994). Researchers who perform experiments and analyses on soil that result in the existence of a plateau on the stress-strain curve and the experimental observation that only one part of the strain is reversible suggest that this framework should be used for constitutive modeling of soils. Plasticity-based models are the most popular for geotechnical materials. The trend for plasticity-based constitutive modeling of soil is to adopt a separate formulation for cohesive and noncohesive soils. In addition, this framework is well adapted to the introduction of constitutive models in computation software based on the finite-element method.

The Drucker-Prager Yield Criterion

The Drucker-Prager yield criterion, formerly known as the extended von Mises yield criterion, forms the basis of one of the most commonly used constitutive models for porous ductile materials

[1]Postgraduate Student, Dept. of Civil Engineering, K. N. Toosi Univ. of Technology, Tehran, Iran. E-mail: jsadoghi@sina.kntu.ac.ir

[2]Assistant Professor, Dept. of Civil Engineering, K. N. Toosi Univ. of Technology, Tehran, Iran. E-mail: fz_kalantary@kntu.ac.ir

[3]Associate Professor, Computer Dept., Ferdowsi Univ. of Mashhad, Mashhad, Iran (corresponding author). E-mail: h-sadoghi@um.ac.ir

Note. This manuscript was submitted on May 27, 2010; approved on May 19, 2011; published online on May 23, 2011. Discussion period open until November 1, 2012; separate discussions must be submitted for individual papers. This paper is part of the ***International Journal of Geomechanics***, Vol. 12, No. 3, June 1, 2012. ©ASCE, ISSN 1532-3641/2012/3-229–238/$25.00.

that are weak in tension and can incorporate hardening because of plastic volumetric strain.

The Drucker-Prager criterion can be perceived as an attempt to create a smooth approximation to the Mohr-Coulomb surface in the same manner as von Mises approximates Tresca (Zienkiewicz et al. 1999). The failure surface is a cone with a circular cross section as shown in Fig. 1.

The Yield Function

In order to derive the elastoplastic stress-strain relationship, better known as the constitutive equations, a number of concepts need to be reiterated:

- The yield surface defines the boundary in the stress space on which the behavior of a material becomes plastic (irreversible).
- The elastic domain defines the boundary in the stress space interior to the yield surface; inside the elastic domain, strains remain reversible.
- The yield function, the boundary of the elastic domain, is defined in practice by a scalar function F of the stress tensor, where $F(\sigma_{ij})$ is the yield function. In the principle stress space (σ_{11}, σ_{22}, σ_{33}), the yield function $F(\sigma_{ij})$ is given by

$$F(\sigma_{ij}) = \sqrt{J_2} - \alpha I_1 - k = 0 \tag{1}$$

where I_1 and J_2 = first invariant of the stress tensor σ_{ij} and second invariant of the deviatoric stress tensor s_{ij}, respectively, and

$$I_1 = \sigma_{11} + \sigma_{22} + \sigma_{33} \tag{2}$$

$$J_2 = \frac{1}{6}[(\sigma_{11} - \sigma_{22})^2 + (\sigma_{11} - \sigma_{33})^2 + (\sigma_{22} - \sigma_{33})^2] \tag{3}$$

where α and k = material constants, which make the Drucker-Prager circle coincide with the outer apices of the Mohr-Coulomb hexagon at any section by relating the Coulomb material parameters c and φ, which are the cohesion and angle of internal friction, respectively (Mestat et al. 2008).

For the triaxial compression test ($\sigma_{11}, \sigma_{22} = \sigma_{33}$), constants α and k are

$$\alpha = \frac{2\sin\varphi}{\sqrt{3}(3 - \sin\varphi)} \tag{4}$$

$$k = \frac{6c \cdot \cos\varphi}{\sqrt{3}(3 - \sin\varphi)} \tag{5}$$

The sign of the yield function defines the position of a given stress state. Using the yield function, the elastic-plastic behavior (loading criteria) and elastic behavior (unloading criteria) are expressed as

$$\begin{cases} F(\sigma_{ij}) < 0: & & & \text{elastic behavior} \\ F(\sigma_{ij}) = 0 & \text{and} & dF > 0: & \text{elastic} - \text{plastic behavior} \\ F(\sigma_{ij}) = 0 & \text{and} & dF < 0: & \text{elastic behavior} \end{cases} \tag{6}$$

In the elastic state, for computation of total strain (ε) per stress (σ), the following equation is defined:

$$d\varepsilon_{ij} = C^e \cdot d\sigma_{ij} \tag{7}$$

Eq. (7) is then expressed as

$$\begin{bmatrix} d\sigma_{xx} \\ d\sigma_{yy} \\ d\sigma_{zz} \\ d\sigma_{xy} \\ d\sigma_{yz} \\ d\sigma_{xz} \end{bmatrix} = \frac{E}{(1+\nu)(1-2\nu)} \begin{bmatrix} 1-\nu & \nu & \nu & 0 & 0 & 0 \\ \nu & 1-\nu & \nu & 0 & 0 & 0 \\ \nu & \nu & 1-\nu & 0 & 0 & 0 \\ 0 & 0 & 0 & \frac{1-2\nu}{2} & 0 & 0 \\ 0 & 0 & 0 & 0 & \frac{1-2\nu}{2} & 0 \\ 0 & 0 & 0 & 0 & 0 & \frac{1-2\nu}{2} \end{bmatrix} \begin{bmatrix} d\varepsilon_{xx} \\ d\varepsilon_{yy} \\ d\varepsilon_{zz} \\ d\varepsilon_{xy} \\ d\varepsilon_{yz} \\ d\varepsilon_{xz} \end{bmatrix} \tag{8}$$

where parameters E and ν = modulus of elasticity and the Poisson's ratio, respectively.

In the elastoplastic state, for computation of total strain rate ($d\varepsilon$) with respect to stress rate ($d\sigma$), the following equation is defined:

$$d\varepsilon_{ij} = d\varepsilon_{ij}^e + d\varepsilon_{ij}^p = (C^e + C^p) \cdot d\sigma_{ij} \tag{9}$$

The plastic strain increments are related to the flow rule. By considering the associated flow rule, using of consistency condition, and defining parameter H, which is expressed as

$$H = -\left(\frac{\partial F}{\partial \varepsilon_{ij}^p}\right)^T \left(\frac{\partial F}{\partial \sigma_{ij}}\right) \tag{10}$$

and computing the H parameters, the plastic strain increment is expressed as

$$\begin{bmatrix} d\varepsilon_{xx}^p \\ d\varepsilon_{yy}^p \\ d\varepsilon_{zz}^p \\ d\varepsilon_{xy}^p \\ d\varepsilon_{yz}^p \\ d\varepsilon_{xz}^p \end{bmatrix} = \frac{1}{H} \begin{bmatrix} \frac{\partial F(\sigma_{ij})}{\partial \sigma_{xx}} \\ \frac{\partial F(\sigma_{ij})}{\partial \sigma_{yy}} \\ \frac{\partial F(\sigma_{ij})}{\partial \sigma_{zz}} \\ \frac{\partial F(\sigma_{ij})}{\partial \sigma_{xy}} \\ \frac{\partial F(\sigma_{ij})}{\partial \sigma_{yz}} \\ \frac{\partial F(\sigma_{ij})}{\partial \sigma_{xz}} \end{bmatrix} \begin{bmatrix} \frac{\partial F(\sigma_{ij})}{\partial \sigma_{xx}} & \frac{\partial F(\sigma_{ij})}{\partial \sigma_{yy}} & \frac{\partial F(\sigma_{ij})}{\partial \sigma_{zz}} & \frac{\partial F(\sigma_{ij})}{\partial \sigma_{xy}} & \frac{\partial F(\sigma_{ij})}{\partial \sigma_{yz}} & \frac{\partial F(\sigma_{ij})}{\partial \sigma_{xz}} \end{bmatrix} \tag{11}$$

Because ε_{ij}^p and H are interdependent, to obtain ε_{ij}^p, generally a function must be assumed for their correlation. However, the adopted optimization method here circumvents this by evaluating H locally.

Int. J. Geomech., 2012, 12(3): 229-238

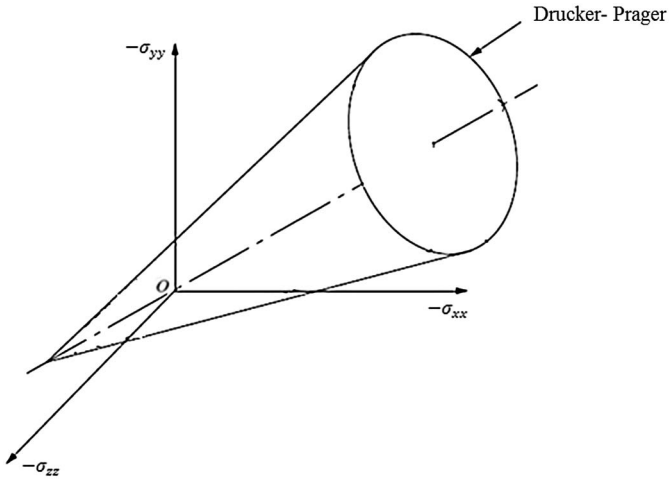

Fig. 1. Yield surface corresponding to the Drucker-Prager criterion

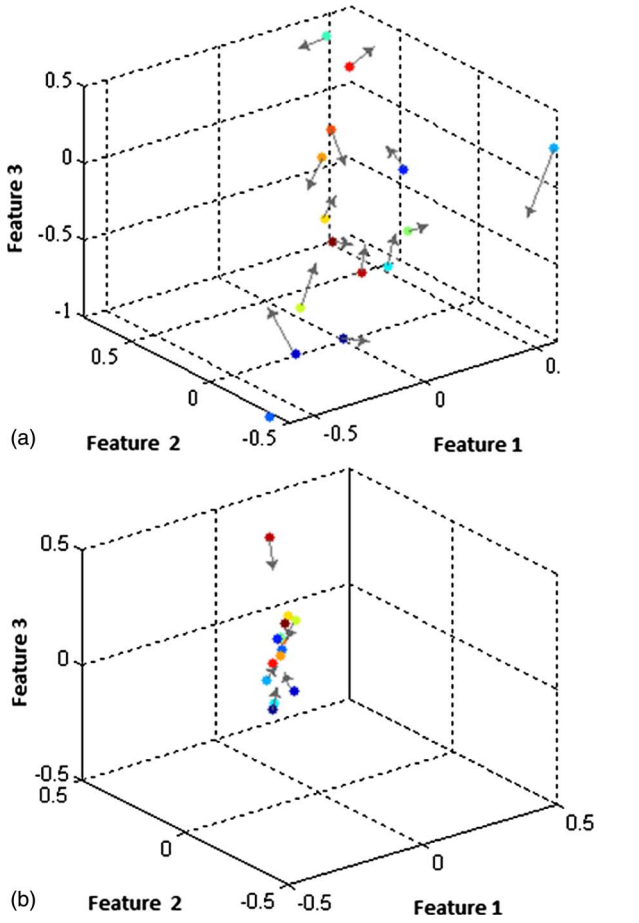

Fig. 2. Direct and velocity particles in the search space with three features: (a) initial movement; (b) advance movement

Particle Swarm Optimization

Kennedy and Eberhart (1995) introduced the PSO algorithm for the first time as a new population-based optimization technique inspired by animal social behavior.

In the PSO algorithm, each individual particle flies in the search space with a velocity that is dynamically adjusted according to its own flying experience and its companions' flying experiences. The PSO algorithm possesses some attractive properties such as memory and constructive cooperation between individuals. Thus, it has more chances to fly into better solution areas more quickly and discover a reasonable quality solution much faster, and no selection and crossover operator exist (Kennedy and Eberhart 1995). In Fig. 2(a), each particle is randomly positioned in the search space and thus has its own position and initial velocity so any particle can move to any part of the search space. This velocity is controlled by the movement imposed on the particle, changing its spatial location in search of a better performance. Therefore, with these movements the particles converge to the optimum location in the search space and all of the particles tend to move to a specific point [see Fig. 2(b)].

Further explanation on the PSO algorithm and its usage in various fields may be found in Mirghasemi et al. (2010). Here, PSO is used for optimization of soil parameters over Drucker-Prager yield criteria. Details of the search procedure with PSO are mentioned in the next section.

Neuro-Fuzzy Inference System

Recently, there has been a growing interest in combining both these approaches, and as a result, neuro-fuzzy computing techniques have evolved. Neuro-fuzzy systems are fuzzy systems that use neural network theory to determine their properties (fuzzy sets and fuzzy rules) by processing data samples (Mitra and Hayashi 2000). Neuro-fuzzy integrates to synthesize the merits of both neural networks and fuzzy systems in a complementary way to overcome their disadvantages. The fusion of a neural network and fuzzy logic into neuro-fuzzy models yields low-level learning, the computational power of neural networks, and the advantages of high-level humanlike thinking of fuzzy systems. The adaptive network based on fuzzy inference system (ANFIS) model combined the neural network adaptive capabilities and the fuzzy logic qualitative approach initially introduced by Jang (1993).

In recent years, ANFIS has attained popularity because of its adaptability in a broad range of useful applications in such diverse areas as optimization of fishing predictions (Iglesias Nuno et al. 2005), vehicular navigation (Noureldin et al. 2007), identification of turbine speed dynamics (Kishor et al. 2007), radiofrequency power amplifier linearization (Lee and Gardner 2006), microwave applications (Ubeyli and Guler 2006), image de-noising (Qin and Yang 2007; Çivicioglu 2007), predictions in cleaning with high-pressure water (Daoming and Jie 2006), sensor calibration (Depari et al. 2007), fetal electrocardiogram (ECG) extraction from ECG signals captured from the mother (Assaleh 2007), and identification of normal and glaucomatous eyes (Huang et al. 2007). Also, previous works of the writers (Sadoghi Yazdi and Pourreza 2010) in the field of ANFIS architecture on solutions of ordinary differential equations, constraint modeling, and control are available.

All of these works show that ANFIS is a good universal approximator, predictor, interpolator, and estimator, and demonstrates that ANFIS has the approximation capabilities of neural networks. Any nonlinear function of several inputs and outputs can be easily constructed with ANFIS. The advantages of the ANFIS technique are summarized as follows:

- Real-time processing of instantaneous system input and output data. This property helps when using this technique for many operational research problems.
- Offline adaptation instead of online system-error minimization; thus, it is easier to manage and no iterative algorithms are involved.
- System performance is not limited by the order of the function because it is not represented in polynomial format.
- Fast learning time.

Int. J. Geomech., 2012, 12(3): 229-238

- System performance tuning is flexible as the number of membership functions and training epochs can be altered easily.
- The simple if/then rules declaration and the ANFIS structure are easy to understand and implement.

On the other hand, numerous problems in science and engineering can be explained through a form of system identification or regression. Basic methods can be achieved to identification problems and regression as neural networks and neuro-fuzzy models. In this paper, the neuro-fuzzy model is used for system identification.

Proposed Method

The overall procedure for evaluation of the basic soil parameters (i.e., E, ν, c, and φ) and other variables calculated during the procedure (such as the coefficients of the hardening law) are presented in Fig. 3.

Initially, an ANFIS was used to arrive at a nonlinear regression of the available test result. Then, the required parameters needed to produce the results were randomly set and used in the simultaneous solution of the Eqs. (1)–(11) for each increment of loading. The solutions will produce errors (residuals) with respect to the ANFIS model. If the amount of the error exceeded a predetermined criterion (e.g., 1%) the parameters were reevaluated using PSO and re-fed into the equations for a new solution. Further explanation on each step of the algorithm is provided below.

ANFIS Model

Basically, the ANFIS model guides the search mechanism of PSO. First, the stress generator produces deviatoric stresses within the range of the experimental data. Then, the model predicts the appropriate strain (Fig. 4).

The structure of the ANFIS model is shown in Fig. 5, in which the circles indicate fixed nodes, and the squares indicate adaptive nodes. Considering inputs x and one output z in the fuzzy inference system (FIS), the ANFIS implements a first-order Sugeno fuzzy model. Among the many FISs, the Sugeno fuzzy model is the most widely used because of its high interpretability, computational efficiency, and built-in optimal and adaptive techniques. For example, for a first-order Sugeno fuzzy model, a common rule set with two fuzzy if/then rules can be expressed as follows (where cluster $i = 1, \ldots, 5$ are fuzzy sets in the antecedent as shown in Fig. 6 and the parameters are determined during the training process):

- Rule 1: if deviatoric stress is Cluster 1, then $z_1 = -2.212$ and deviatoric stress = 87.62.
- Rule 2: if deviatoric stress is Cluster 2, then $z_2 = -117.4$ and deviatoric stress = 1.021×10^4.
- Rule 3: if deviatoric stress is Cluster 3, then $z_3 = -37.48$ and deviatoric stress = 2,375.
- Rule 4: if deviatoric stress is Cluster 4, then $z_4 = -41.6$ and deviatoric stress = 6,290.
- Rule 5: if deviatoric stress is Cluster 5, then $z_5 = 0.001673$ and deviatoric stress = -9.277×10^{-6}.

The ANFIS consists of five layers (see Fig. 5). In Layer 1, every node i is an adaptive node with a node function

$$O_i^2 = \mu_{A_i}(x)_0 \quad i = 1, \ldots, 5 \tag{12}$$

where x = input of node i, and $\mu_{A_i}(x)$ can adopt any fuzzy membership function (MF). Here, Gaussian MFs are used as follows:

$$\text{Gaussian}\ (x, c, \sigma) = e^{-(1/2)[(x-c)/\sigma]^2} \tag{13}$$

where c = center of Gaussian membership function and σ = standard deviation of this cluster as shown in Table 1.

In Layer 2, every node represents the ring strength of a rule by multiplying the incoming signals and forwarding the product as

$$O_i^2 = \omega_i = \mu_{A_i}(x) \quad i = 1, \ldots, 5 \tag{14}$$

In Layer 3, the ith node calculates the ratio of the ith rule's ring strength to the sum of all rules' ring strengths

$$O_i^3 = \bar{\omega}_i = \frac{\omega_i}{\sum_{j=1}^{5} \omega_j} \quad i = 1, \ldots, 5 \tag{15}$$

where $\bar{\omega}_i$ = normalized ring strengths. In Layer 4, the node function is represented by

Fig. 4. ANFIS model of stress per strain

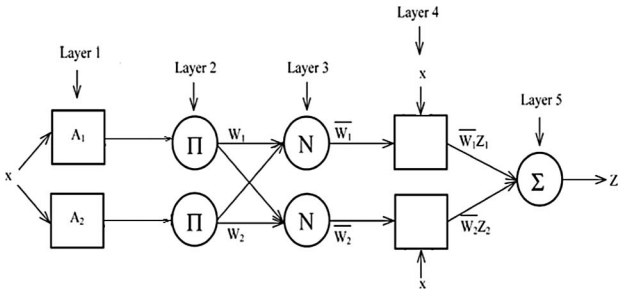

Fig. 5. ANFIS architecture [Π, N, and Σ are defined in Eqs. (15), (16), and (18), respectively]

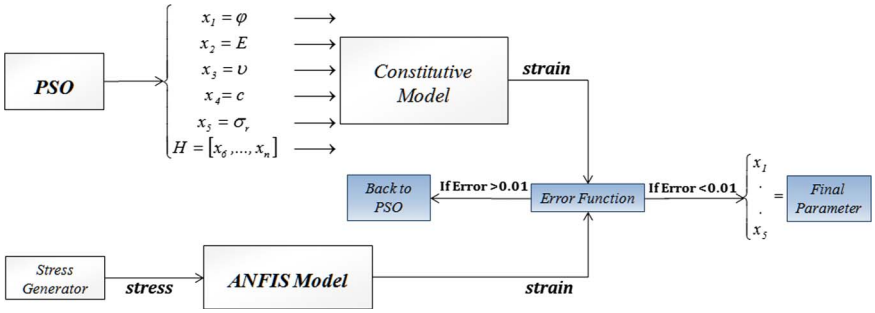

Fig. 3. Proposed structure

Int. J. Geomech., 2012, 12(3): 229-238

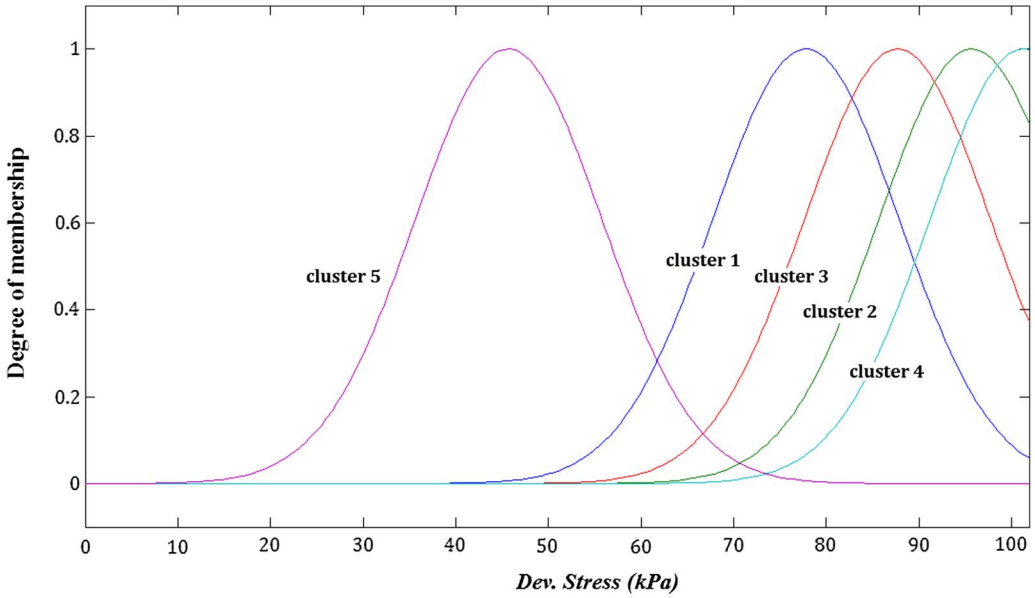

Fig. 6. Fuzzy sets of input variables [degree of membership per deviatoric stress (kPa)]

Table 1. Center and Standard Deviation of Gaussian Membership Function

Cluster	1	2	3	4	5
Deviatoric stress (standard deviation)	10.1	10.09	10.09	10.09	10.09
Center	77.5	87.69	95.72	101.3	45.7

$$O_i^4 = \bar{\omega}_i Z_i = \bar{\omega}_i (p_i x + r_i), \qquad i = 1, \ldots, 5 \tag{16}$$

where $\bar{\omega}_i$ = output of Layer 3, and $\{p_i, r_i\}$ = aforementioned parameter rule set and is shown in Table 2. The parameters in this layer are referred to as the consequent parameters.

In Layer 5, the single node computes the overall output as the summation of all incoming signals as follows:

$$O_i^5 = \sum_{i=1}^{5} \bar{\omega}_i z_i = \frac{\sum_{i=1}^{5} \omega_i z_i}{\sum_{i=1}^{5} \omega_i} \tag{17}$$

It is seen from the ANFIS architecture that when the values of the premise parameters are fixed, the overall output can be expressed as a linear combination of the consequent parameters

$$z = \bar{\omega}_1 p_1 x + \bar{\omega}_1 r_1 + \bar{\omega}_2 p_2 x + \bar{\omega}_2 r_2 + \cdots + \bar{\omega}_5 p_5 x + \bar{\omega}_5 r_5 \quad \text{or}$$
$$z = (\omega_1 p_1 + \omega_2 p_2 + \cdots + \omega_5 r_5) x + (\omega_1 r_1 + \omega_2 r_2 + \cdots + \omega_5 r_5) \tag{18}$$

The hybrid learning algorithm (Jang 1993; Depari et al. 2007), which combines the least-squares method and the back-propagation (BP) algorithm, can be used to solve this problem. This algorithm converges much faster because it reduces the dimension of the search space of the BP algorithm. During the learning process, the premise parameters in Layer 1 and the consequent parameters in Layer 4 are tuned until the desired response of the FIS is achieved. The hybrid learning algorithm has a two-step process. First, while holding the premise parameters fixed, the functional signals are propagated forward to Layer 4, where the consequent parameters are identified by the least-squares method. Second, the consequent parameters are held fixed while the error signals (the derivative of the error measure with respect to each node output) are propagated from the output end to the input end, and the premise parameters are updated by the standard BP algorithm.

Table 2. Parameter Set of Lines $\{p_i, r_i\}$

Cluster	1	2	3	4	5
p_i	−2.212	−117.4	−37.48	−41.6	0.001673
r_i	87.62	10210	2375	6290	−9.3*E*-06

Noise Robustness

One of abilities of the ANFIS model is noise robustness, which can be discovered with signal-to-noise ratio (SNR) in the following form:

$$\text{SNR} = 20 \log \left(\frac{D_s}{D_n} \right) \tag{19}$$

where D_s = signal domain and D_n = noise domain. Fitting the operation with different SNRs is compared with the noiseless condition. Fig. 7 shows the 46 dB noisy condition and the noiseless state. Also, the error between the base curve (noiseless condition) and the fitted curve in the noisy condition is defined as

$$E_{\text{SNR}} = \frac{1}{L} \sqrt{\sum_{i=1}^{n} [Z_b(i) - Z_{\text{SNR}}(i)]^2} \tag{20}$$

where E_{SNR} = error when comparing the base output $[Z_b(i)]$ and the output in the noisy condition $[Z_{\text{SNR}}(i)]$; L = length of signal; and n = number of the sample entered into the error calculation.

The results confirming the robustness of the ANFIS model against noise are shown in Fig. 8. Also, for example, when SNR = 10 dB or the domain of noise is 60%, the signal domain obtained error is 11%. In this example, training samples are shown in Fig. 9. The result of the fitting procedure by ANFIS is shown in Fig. 10.

Int. J. Geomech., 2012, 12(3): 229-238

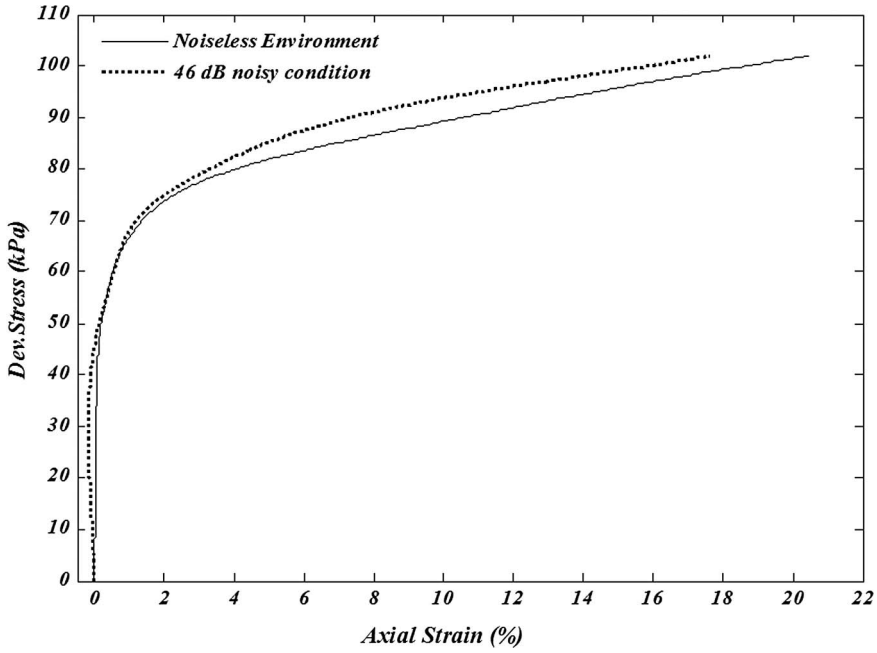

Fig. 7. Comparison of the fitting operation in the noiseless environment and the 46 dB noisy condition

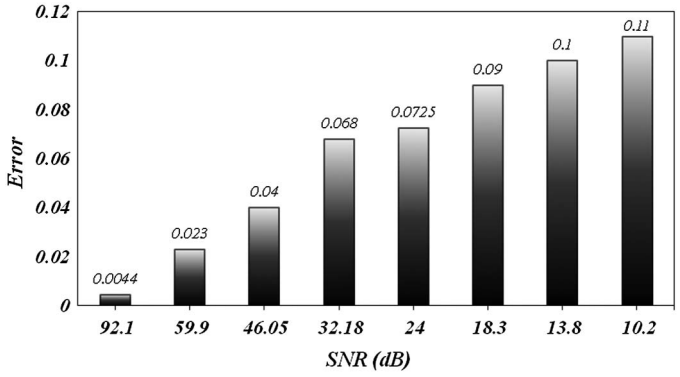

Fig. 8. Estimated error under different noise conditions

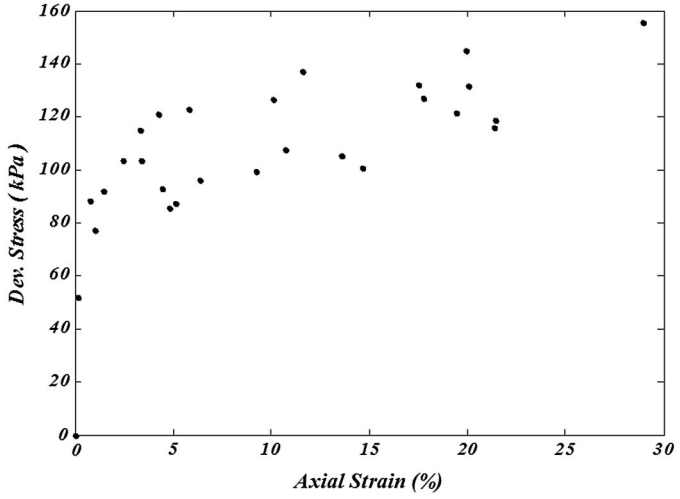

Fig. 9. Training samples for the SNR = 10.2 dB condition

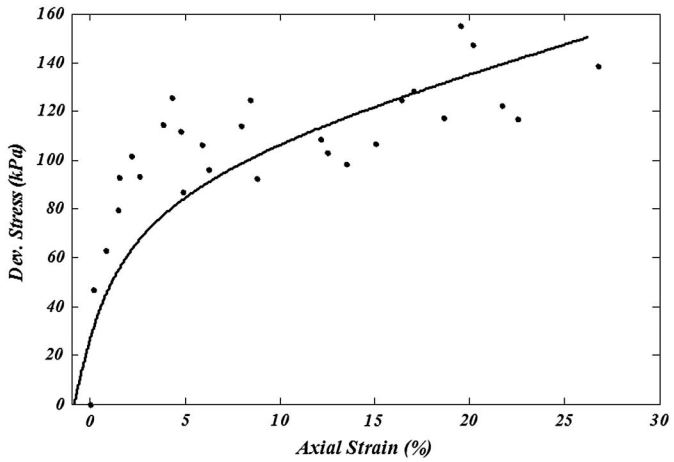

Fig. 10. Fitted curve in the SNR = 10 dB condition

The observed data from the triaxial test and the neuro-fuzzy model are shown in Fig. 11.

Solving with PSO

In this section, the method for evaluation of the soil parameters used in the aforementioned elastoplastic model with the PSO search algorithm in conjunction with the ANFIS model is introduced. The overall structure of the algorithm in the form of an iterative convergence loop is schematically shown in Fig. 12.

To evaluate an increment of the axial strain with respect to the deviatoric stress increment, the vector of the main parameters $x_i = [x_1, x_2, \cdots, x_5]^T = [\varphi, E, \nu, c, \sigma_r]^T$ is fed into the constitutive equations. If the load increment did not cause plastic straining, the calculations remained within the bound of elasticity and only the appropriate parameters were evaluated. However, when plastic

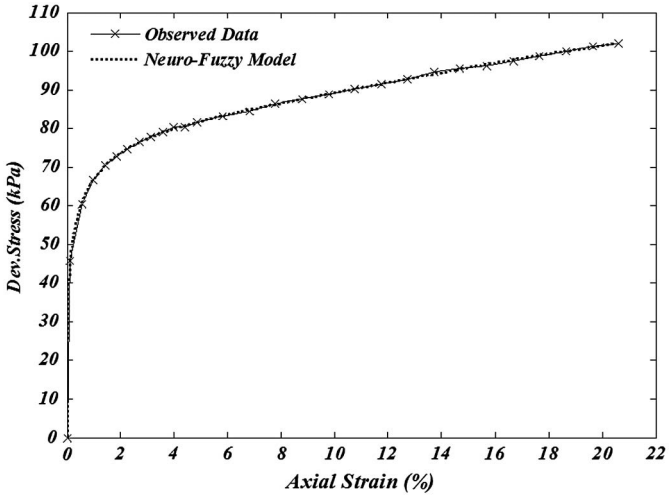

Fig. 11. Results of the neuro-fuzzy model

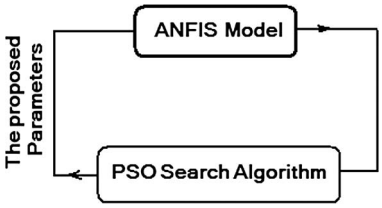

Fig. 12. Simple form of the proposed method

straining did occur, Eqs. (9)–(11) were also invoked and, in doing so, the hardening parameter needed to be locally evaluated.

The estimated values of the strains were compared against the model produced by ANFIS, the error was evaluated, and the outcome was dealt with according to the acceptance criterion. If the outcome had an unacceptable error, the following procedure (Fig. 13), which included six main steps, was carried out to arrive at a better answer:

1. Initialization of PSO;
2. Evaluation of particle position and velocity updating;
3. Velocity weight adaptation;
4. Personal and global best location;

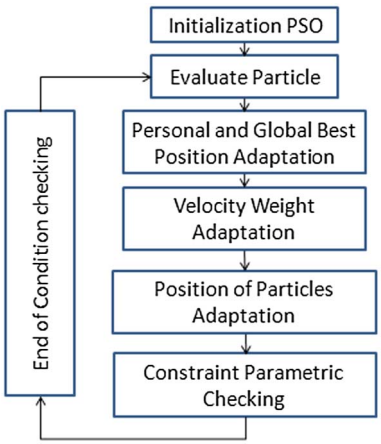

Fig. 13. PSO algorithm for soil parameter optimization

5. Location particles adaptation and constraint parametric checking; and
6. End of condition checking.

The PSO algorithm will be described in the following section.

Initialization PSO and Definition

The initialization position (particle X) and associated velocity ($\text{particle}_j^i \cdot v$) of all particles were randomly set to within prespecified values in the feasible region where $\text{particle}_j^i \cdot X = [x_i]$ (see Fig. 3). $\text{particle}_j^i \cdot v$ is the velocity of any $\text{particle}_j^i \cdot X$. The best state of the ith particle in the jth iteration is represented by the $\text{particle}_j^i \cdot \text{best}$ structure and the best particle in the population is represented by $\text{best}_j \cdot \text{particle}$.

Evaluate Error Index

Evaluation of the error index (total error value) of all particles was done with the following error function:

$$E_{\text{PSO}} = \frac{1}{m}\sum_{i=1}^{m}(\varepsilon_{(\text{ANFIS})} - \varepsilon_{(\text{PSO})})^2 \tag{21}$$

where m = number of particles; $\varepsilon_{(\text{ANFIS})}$ = strain obtained by the ANFIS model; and $\varepsilon_{(\text{PSO})}$ = strain obtained by feeding the PSO determined parameters into the set of constitutive equations.

Personal and Global Best Position

$\text{particle}_j^i \cdot \text{best}$ represents the minimum error value of the nth particle. The $\text{particle}_j^i \cdot \text{best}$ error of each particle was compared with the current total error value calculated by Eq. (21). If the current total error value was less, the current error value was assigned to the $\text{particle}_j^i \cdot \text{best} \cdot \text{error}$ least error and the current coordinates were assigned to $\text{particle}_i \cdot \text{best} \cdot X$. In a similar way, the least error value in the entire population and its coordinates can be determined. If the current error is less than the best particle, then assign the current coordinates to the best particle and assign the current error value to $\text{particle}_j^i \cdot \text{best} \cdot \text{error}$, where the best particle represents the best particle in the total population.

Velocity Weight Adaptation

The velocity weight can be changed using the following rule:

$$\begin{aligned}\text{particle}_{j+1}^i \cdot v = {} & \alpha_p \times \text{particle}_j^i \cdot v + C_1 \times U_1 \\ & \times (\text{particle}_j^i \cdot \text{best} \cdot X - \text{particle}_j^i \cdot X) + C_2 \times U_2 \\ & \times (\text{best}_j \cdot \text{particle} \cdot X - \text{particle}_j^i \cdot X)\end{aligned} \tag{22}$$

where $C_1 = C_2 = 0.5$ = factors used to control the related weighing of corresponding terms; U_1 and U_2 = random variables from the range [0,1]; α_p = parameter controlling the dynamics of flying; and the balance between the global and local search is adjusted through the parameter $\alpha_p \in (0, \infty)$.

Position Particle Adaptation and Constraint Parametric Checking

Change the position using the following rule:

$$\text{particle}_{j+1}^i \cdot X = \text{particle}_j^i \cdot X + \text{particle}_j^i \cdot v \tag{23}$$

After updating the model, $\text{particle}_{j+1}^i \cdot X$ would also be checked and clamped to the legal range to ensure a legal solution; if a particle was removed from the feasible region, then it would be returned to the border of the feasible region.

End of Condition Checking

Repeat Steps 2–6 until a stop criterion is satisfied or a predefined number of iterations is completed. This algorithm is run twice, once

Int. J. Geomech., 2012, 12(3): 229-238

to calculate Eq. (1) until the Eq. (11) result of the above algorithm is $x_i = [x_1, \ldots, x_5]^T$.

Determination of the Soil Parameter with PSO

The test result was initially simulated with a limited number of particles (i.e., 100). This produced a stress-strain curve with large inaccuracies [see Fig. 14(a)]. Thus, the number of particles was increased to 1,500 (vectors), which produced a very close fit [see Fig. 14(b)]. The obtained parameters using PSO that would simulate the above behavior are shown in Table 3.

To provide another angle to the procedure, the data from a second test on the same sand with a confining pressure of 100 kPa were also used to calibrate the model parameters. The outcome was very close to the first run, with the same order of accuracy.

The results of the ANFIS model together with the PSO simulation for the second test are shown in Fig. 15 and the outcome of the analysis is presented in Table 4. It can be seen that in spite of the notable discrepancy in the prediction of the confining pressure the technique is capable of capturing the essence of the test condition.

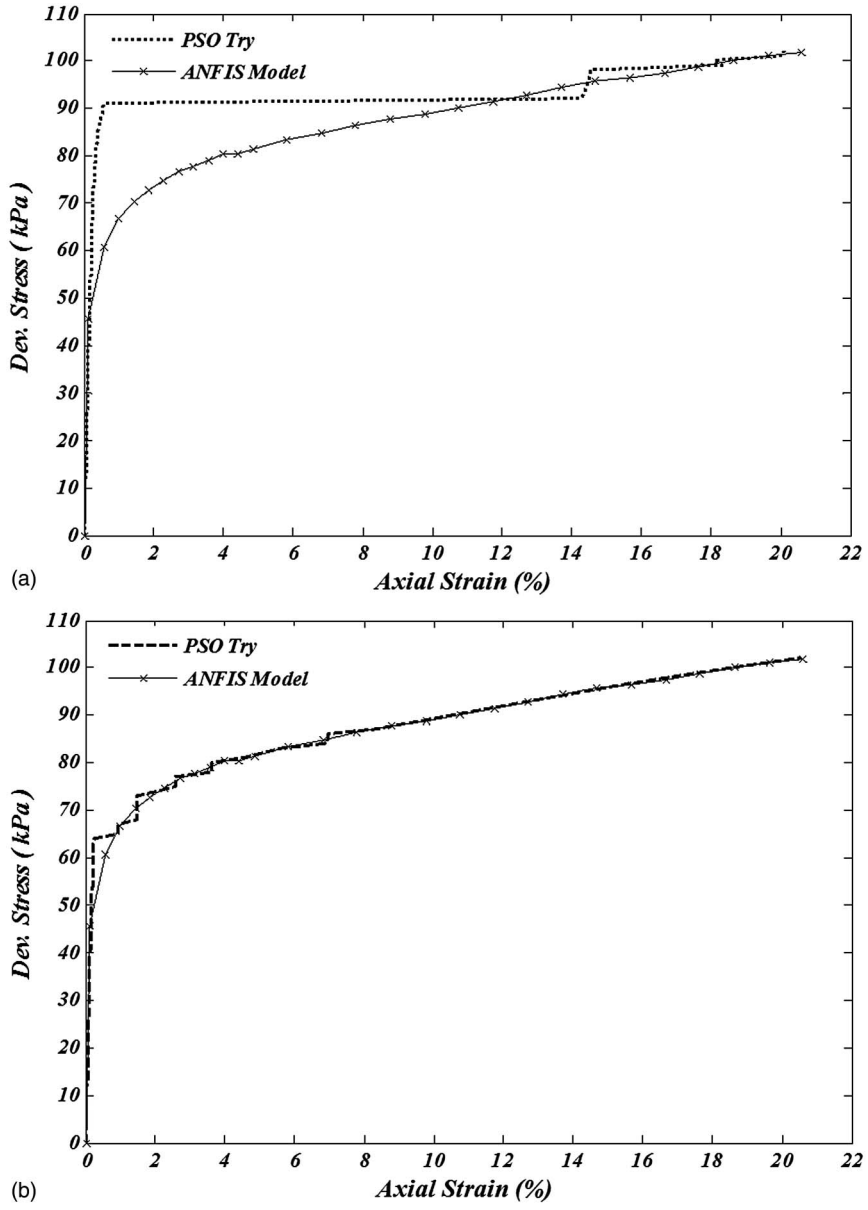

Fig. 14. (a) PSO search step; (b) developed search procedure using PSO

Table 3. Estimated Values of the Model Parameters

Model	Internal friction angle (φ)	Module of elasticity	Poisson ratio (υ)	Cohesion	Radial stress
PSO derived	30.31°	300.013 kPa	0.35	0.192 kPa	25.017 kPa
Experiment	36.38°	Not measured	Not measured	0	50 kPa

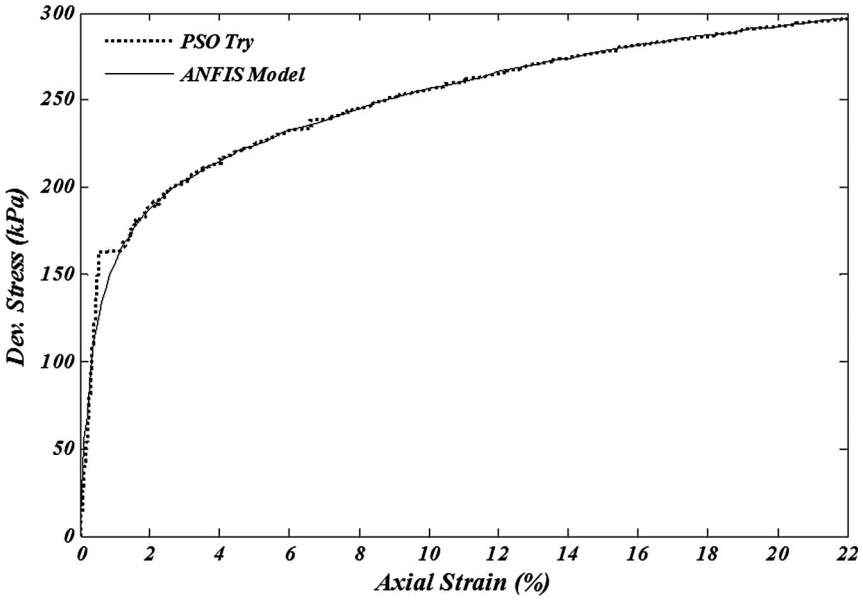

Fig. 15. Results of the second test with a confining pressure of 100 kPa

Table 4. Prediction of the Basic Model Parameters for the Second Test

Internal friction angle (φ)	Module of elasticity	Poisson ratio (υ)	Cohesion	Radial stress
30.216°	300.001 kPa	0.3498	1.410 kPa	78.286 kPa

Summary and Conclusions

Calibration of constitutive models requires close examination of extensive experimental data. Even then, some of the more intricate parameters deployed in the more advanced and complicated models cannot simply be correlated to any experimentally measured properties and often simplifying assumptions have to be made.

The technique described in this paper has proven its capabilities as an identification procedure in many fields, including geomechanics. However, its versatility in calibration of model parameters as well as peripheral variables from the very basic and minimal experimental data can be viewed as a potent tool in the development of constitutive models. This capability was demonstrated using a simple model with the most meager data. Obviously, further exploration of the technique with more extensive data can lead to better approximations for more complex models.

Notation

The following symbols are used in this paper:

D_n = noise domain;
D_s = signal domain;
E = module of elasticity;
E_{PSO} = error function of PSO;
E_{SNR} = error of SNR;
I_1 = first invariant of stress tensor;
J_2 = second invariant of deviatoric stress tensor;
k = material constant;
L = length of signal;
m = number of particle;
n = number of sample;
p_i, r_i = parameter set of lines;
U_1, U_2 = random variables;
$Z_b(i)$ = base output;
$Z_{\mathrm{SNR}}(i)$ = noisy condition;
α = material constant;
α_p = parameter controlling the dynamics of flying;
$\varepsilon_{(\mathrm{ANFIS})}$ = strain obtained by ANFIS model;
$\varepsilon_{(\mathrm{PSO})}$ = strain obtained by feeding PSO;
ε_{ij}^{P} = plastic strain tensor;
$\mu_{A_i}(x)$ = Gaussian membership function;
ν = Poisson ratio;
σ_{ij} = stress tensor; and
$\bar{\omega}_i$ = normalized ring strength.

References

Assaleh, K. (2007). "Extraction of fetal electrocardiogram using adaptive neuro-fuzzy inference systems." *IEEE Trans. Biomed. Eng.*, 54(1), 59–68.

Chen, W.-F. (1994). *Constitutive equations for engineering materials*, Vol. 2, Elsevier Science, Amsterdam, Netherlands.

Çivicioglu, P. (2007). "Using uncorrupted neighborhoods of the pixels for impulsive noise suppression with ANFIS." *IEEE Trans. Image Process.*, 16(3), 759–773.

Cui, L., and Sheng, D. (2005). "Genetic algorithms in probabilistic finite element analysis of geotechnical problems." *Comput. Geotech.*, 32(8), 555–563.

Daoming, G., and Jie, C. (2006). "ANFIS for high-pressure waterjet cleaning prediction." *Surf. Coat. Technol.*, 201(3-4), 1629–1634.

Depari, A., Marioli, A. D., and Taroni, A. (2007). "Application of an ANFIS algorithm to sensor data processing." *IEEE Trans. Instrum. Meas.*, 56(1), 75–79.

Feng, X.-T., Chen, B.-R., Yang, C., Zhou, H., and Ding, X. (2006). "Identification of visco-elastic models for rocks using genetic programming coupled with the modified particle swarm optimization algorithm." *Int. J. Rock Mech. Min. Sci.*, 43(5), 789–801.

Finsterle, S. (2006). "Demonstration of optimization techniques for groundwater plume remediation using iTOUGH2." *Environ. Modell. Software*, 21(5), 665–680.

Huang, M.-L., Chen, H.-Y., and Huang, J.-J. (2007). "Glaucoma detection using adaptive neuro-fuzzy inference system." *Expert Syst. Appl.*, 32(2), 458–468.

Iglesias Nuno, A., Arcay, B., Cotos, J. M., and Varela, J. (2005). "Optimisation of fishing predictions by means of artificial neural networks, ANFIS, functional networks and remote sensing images." *Expert Syst. Appl.*, 29(2), 356–363.

Jang, J. S. R. (1993). "ANFIS: Adaptive-network-based fuzzy inference system." *IEEE Trans. Syst. Man Cybern.*, 23(3), 665–685.

Kennedy, J., and Eberhart, R. (1995). "Particle swarm optimization." *Proc., IEEE Int. Conf. on Neural Networks*, Vol. 4, Perth, Australia, 1942–1948.

Kishor, N., Singh, S. P., and Raghuvanshic, A. S. (2007). "Adaptive intelligent hydro turbine speed identification with water and random load disturbances." *Eng. Appl. Artif. Intell.*, 20(6), 795–808.

Lee, K. C., and Gardner, P. (2006). "Adaptive neuro-fuzzy inference system (ANFIS) digital predistorter for RF power amplifier linearization." *IEEE Trans. Veh. Technol.*, 55(1), 43–51.

Levasseur, S., Malecot, Y., Boulon, M., and Flavigny, E. (2008). "Soil parameter identification using a genetic algorithm." *Int. J. Numer. Anal. Methods Geomech.*, 32(2), 189–213.

Meier, J., Schaedler, W., Borgatti, L., Corsini, A., and Schanz, T.. (2008). "Inverse parameter identification technique using PSO algorithm applied to geotechnical modeling." *J. Artif. Evol. Appl.*, 2008, 1–14.

Mestat, P., Bourgeois, E., and Reiffsteck, P. (2008). "Elastoplastic modeling of soils: Monotonic loadings." Chapter 3, *Constitutive modeling of soil and rocks*, P.-Y. Hicher and J.-F. Shao, eds., Wiley, Hoboken, NJ, 77–143.

Mirghasemi, S., Sadoghi Yazdi, H., and Lotfizad, M. (2010). "Linear and quadratic PSO based color space conversion for sea target detection." *Int. J. Comput. Electr. Eng.*, 2(1), 111–118.

Mitra, S., and Hayashi, Y. (2000). "Neuro-fuzzy rule generation: Survey in soft computing framework." *IEEE Trans. Neural Netw.*, 11(3), 748–768.

Noureldin, A., El-Shafie, A., and Taha, M. R. (2007). "Optimizing neuro-fuzzy modules for data fusion of vehicular navigation systems using temporal cross-validation." *Eng. Appl. Artif. Intell.*, 20(1), 49–61.

Qin, H., and Yang, S. X. (2007). "Adaptive neuro-fuzzy inference systems based approach to nonlinear noise cancellation for images." *Fuzzy Sets Syst.*, 158(10), 1036–1063.

Sadoghi Yazdi, H., and Pourreza, R. (2010). "Unsupervised adaptive neural-fuzzy inference system for solving differential equations." *Appl. Soft Comput.*, 10(1), 267–275.

Schanz, T., Zimmerer, M., Datcheva, M., and Meier, J. (2006). "Identification of constitutive parameters for numerical models via inverse approach." *Felsbau Rock Soil Eng.*, 24(2), 11–21.

Ubeyli, E. D., and Guler, I. (2006). "Adaptive neuro-fuzzy inference system to compute quasi-TEM characteristic parameters of microshield lines with practical cavity sidewall profiles." *Neurocomputing; Variable Star Bull.*, 70(1–3), 296–304.

Zhao, H.-b., and Yin, S. (2009). "Geomechanical parameters identification by particle swarm optimization and support vector machine." *Appl. Math. Modell.*, 33(10), 3997–4012.

Zienkiewicz, O. C., Chen, A. H. C., Pastor, M., Schrefler, B. A., and Shiomi, T. (1999). *Computational geomechanics*, Wiley, New York.

Int. J. Geomech., 2012, 12(3): 229-238